Analysis of short-to-long term heat flow in GSHP systems based on heat pump power

BniLam, Noori; Al-Khoury, Rafid

DOI
10.1016/j.applthermaleng.2019.114561

Publication date
2020

Document Version
Final published version

Published in
Applied Thermal Engineering

Applied Thermal Engineering 173 (2020) 114561

Contents lists available at ScienceDirect

Applied Thermal Engineering

journal homepage: www.elsevier.com/locate/apthermeng

Analysis of short-to-long term heat flow in GSHP systems based on heat pump power

Noori BniLam[a,b,*], Rafid Al-Khoury[a]

[a] Faculty of Civil Engineering and Geosciences, Computational Mechanics Chair, Delft University of Technology, P.O. Box 5048, 2600 GA Delft, the Netherlands
[b] University of Antwerp – imec, IDLab, Faculty of Applied Engineering, Sint-Pietersvliet 7, 2000 Antwerp, Belgium

HIGHLIGHTS

- A semi-analytical model based on the spectral element method is introduced.
- The model conducts short-to-long term analysis in a single run.
- Hourly, daily and seasonally switching ON and OFF for many years can be considered.
- Heat flow can be calculated based on both Dirichlet and Neumann boundary conditions.
- The Neumann heat flux is derived directly from the heat pump power.

ARTICLE INFO

Keywords:
GSHP
BHE
Spectral element method
Tailored FFT
Shallow geothermal system

ABSTRACT

This paper presents a semi-analytical model based on the spectral element method for three-dimensional, short-to-long term heat flow in multiple borehole, multilayer ground source heat pump systems. The model is distinguished by its computational technique for expressing the input signal at the boundary of the borehole heat exchanger, giving rise to two important engineering features. First, the calculation can be conducted from seconds to years in a single run. This is achieved by discretizing the input signal at the inlet boundary of the borehole heat exchanger using a tailored fast Fourier transform with multiple time-stepping algorithm. Second, the calculation can be conducted using a Neumann boundary condition, instead of the commonly utilized Dirichlet boundary condition. This is achieved by mathematically relating the heat pump power to the heat flux at the inlet of the borehole heat exchanger, allowing direct use of the heat pump power signal as input instead of the inlet temperature. These features make the model computationally efficient that can readily be utilized for system design and included in inverse calculations. The two features are discussed in detail, verified against experimental measurements, and their functionality is highlighted by numerical examples.

1. Introduction

The ground source heat pump (GSHP) technology can play an important role in boosting the economy and improving the environment. It relies on energy gain from shallow depths, which are available nearly everywhere, and its operation produces minimal CO_2 emission into the atmosphere. As a result, this technology is booming, and geothermal engineers are endeavouring to make it more efficient and economic. Several European projects are specifically designed to develop more accurate and reliable computational models aiming to optimize the efficiency of this technology; see for example Horizon2010 Projects [1].

Presently, there are a considerable number of computational models describing heat flow in GSHP systems using different solution methods and adopting a wide range of physical and geometrical complexities. Cui et. al. [2] gave a comprehensive review on the available computational models for GSHP systems. Nevertheless, despite the presence of a large number of models and softwares, there are yet two important engineering features that need to be addressed in a more effective way: short-to-long term analysis of system performance, and analysis directly based on the heat pump power. This paper addresses these two features by introducing a computational technique enabling their implementation within the spectral element framework. Hereafter, we highlight the significance of these two features and how they are treated in this work.

Feature 1: Short-to-long term analysis is important to evaluate the system performance at different times of the days and years. Heating and cooling of buildings includes periods of switching ON and OFF, and

* University of Antwerp – imec, IDLab, Faculty of Applied Engineering, Sint-Pietersvliet 7, 2000 Antwerp, Belgium.
E-mail address: Noori.Bnilam@uantwerpen.be (N. BniLam).

https://doi.org/10.1016/j.applthermaleng.2019.114561
Received 3 May 2019; Received in revised form 11 October 2019; Accepted 17 October 2019
Available online 19 October 2019

during the GSHP lifetime, hourly, daily and seasonal periods of switching ON and OFF take place intensely. This operational requirement severely restricts the calculations such that if detailed transient analysis is sought, the long term performance of the system will be difficult to pursue, but if the global lifetime analysis is sought, the short term performance will be overlooked. As a consequence, the calculations are usually conducted for either short term or long term. This problem is in particular manifested in the numerical models and tools. COMSOL Multiphysics [3], FEFLOW finite element package [4], and, to a lesser extent, ABAQUS finite element package [5] and TOUGH2 finite difference code [6], are the most commonly utilized numerical tools for this purpose. These tools can provide advanced numerical facilities, but are severely restricted in conducting detailed short-to-long term analysis. The demand for a fine mesh due to the geometrical disproportionality of the system and the need for small time steps for the short term analysis make the CPU demands unrealistic for analysing the long term performance of the system, especially if the analysis is intended for daily engineering practice.

Analytical and semi-analytical models are not exemption and the majority of models are mainly suitable for either short term analysis or long term. Attempts to model short-to-long term performance of GSHP systems rely either on the Fast Fourier Transform (FFT) or the step response functions. Marcotte and Pasquier [7], and Zhang et al. [8] introduced, among others, semi-analytical models based on FFT. The FFT algorithm is rather efficient and employing it enables studying the performance of the system for as many time steps as required. However, the standard FFT is formulated for constant time stepping schemes. Depending on the size of the time step, the analysis can go for any desirable time span, yet, only one time step size is allowed: seconds, minutes, hours, days, months or years; not a combination of them. This characteristic restricts the standard FFT from utilization for short-to-long terms analysis; rather for either short term or long term.

Claesson and Javed [9], and Li et al. [10] introduced analytical models to calculate the temperature distribution in the system from minutes to decades. Claesson and Javed [9] adopted a two-step solution. For the short term (the first 100 h) they solve the conductive axial-symmetric heat equation analytically using Laplace transform; and for the long term, they use the line source solution. Li et al. [10], on other hand, developed a temperature response function that combines the composite-medium line-source solution and the conventional ILS and FLS solutions using the matched asymptotic expansion technique. More details on both models can be found in Li et al. [11]. Despite the effectiveness of these models, they are formulated based on the line heat source models which do not take the detailed conduction-convection heat flow in the borehole heat exchanger.

In this paper, we address detailed heat flow in an effectively 3D GSHP systems for short-to-long terms by tailoring the Fast Fourier Transform (FFT) algorithm to allow for the use of multiple time-stepping schemes. This feature facilitates the calculation of heat flow for any desired details, ranging from one second to years, done in a single run.

Feature 2: Analysis based directly on the heat pump power is physically more realistic than that based on a prescribed temperature at the inlet of pipe-in. This temperature is a result of the heat pump operation; i.e. not known a priori. In engineering practice, the heat pump power is prescribed as a heat flux in models solely solving the heat flow in infinite and semi-infinite domains, such as the line and cylindrical

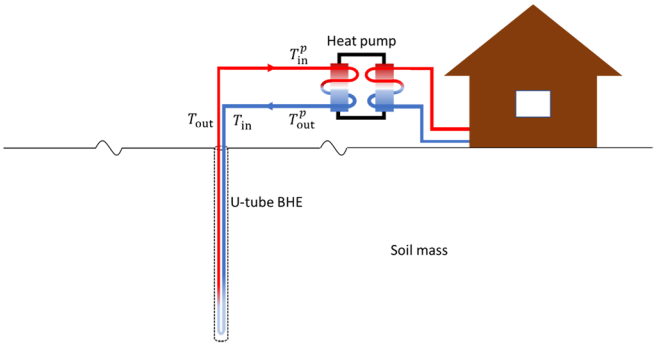

Fig. 1. A schematic representation of a GSHP system.

heat source models. For instance, the heat pump power can directly be prescribed as a constant heat flow rate per unit length, q, in the well-known infinite line source model [12]:

$$T(r, t) \simeq T_0 + \frac{q}{4\pi\lambda_s}\left(\ln\frac{4\alpha t}{r^2} - \gamma\right) \tag{1}$$

in which $T(r, t)$ is the temperature of the medium at radial distance r from the heat line source, λ_s (W/(m K)) is the solid domain thermal conductivity, α(m^2/s) is thermal diffusivity and $\gamma = 0.5772$, Euler's constant.

Models which calculate heat flow in the borehole hole exchanger (BHE), the heat pump power cannot directly be prescribed. Instead, the temperature of the circulating fluid coming out of the heat pump and entering the inlet of pipe-in is prescribed. This temperature is calculated using the power equation:

$$P = \dot{m}c(T^p_{in} - T^p_{out}) \tag{2}$$

in which P(W) is the mean power of the heat pump, $\dot{m}$(kg/s) is the mass flow rate of the circulating fluid, c(J/(kg K)) is its specific heat capacity, T^p_{in}(K) is the fluid temperature entering the heat pump and T^p_{out}(K) is the fluid temperature leaving the heat pump. T^p_{in} is considered equal to the temperature T_{out} coming out of pipe-out of the BHE; and T^p_{out} is considered equal to the temperature T_{in} entering pipe-in of the BHE, see Fig. 1. T_{in} is utilized as the Dirichlet boundary condition to the inlet of pipe-in from which the temperature distribution in the GSHP system is calculated. The procedure to calculate T_{in} from the heat pump power is given in Algorithm 1.

Algorithm 1 (*Prescribing T_{in} based on heat pump power*).

1: DO $n = 1$ to N (n: the time step)
2: Read ${}^{n+1}P$; $\dot{m}$; c
3: Calculate ${}^{n+1}T^P_{out}$ from Eq. (2) such that ${}^{n+1}P = \dot{m}c({}^{n}T^p_{in} - {}^{n+1}T^p_{out})$, (where ${}^{n}T^p_{in}$ is known from the previous time step)
4: ${}^{n+1}T_{in} \leftarrow {}^{n+1}T^P_{out}$
5: Calculate GSHP temperature using ${}^{n+1}T_{in}$ as a prescribed temperature at the inlet of pipe-in
6: Calculate ${}^{n+1}T_{out}$
7: ${}^{n+1}T^P_{in} \leftarrow {}^{n+1}T_{out}$
8: END DO

This algorithm has been implemented in several numerical tools, see for example Al-Khoury et al. [13], Ozudogru et al. [14] and Rui et al. [15]. A similar algorithm is utilized in semi-analytical tools such as EED [16,17] and GLHEPRO [18,19]. Despite the practical use of this algorithm, it suffers the shortcomings of the step response function in terms of its computational inefficiency and the overlooking of the details within the time steps.

In this paper we address the use of heat pump power as a Neumann boundary condition by formulating a mathematical equation relating the heat pump power to the heat flux at the inlet of pipe-in. This feature allows the direct use of heating and cooling design specifications to calculate the temperature distribution in the system. In this case, T_{in} becomes unknown and needs to be computed, similar to T_{out} and all other temperatures at any geometrical point in the system.

2. Theoretical background of the model

The above mentioned two engineering features, short-to-long term analysis and analysis based on the heat pump power, are implemented in the computer code STAND, which stands for **S**hallow geo**T**hermal **A**nalysis a**N**d **D**esign. This code constitutes a semi-analytical spectral element model capable of computing detailed heat flow in effectively three-dimensional GSHPs constituting multiple BHEs embedded in multilayer systems, subjected to arbitrary temporal Neumann or Dirichlet boundary conditions.

The background theory of this model has been thoroughly presented in a string of publications, mainly Al-Khoury [20], BniLam and Al-Khoury [21,22] and BniLam et al. [23]. In Appendix A, we briefly present the governing equations and boundary conditions, together with the resulting spectral element equation necessary for utilization in the follow up sections.

3. Tailored fast Fourier transform

The fast Fourier transform (FFT) entails transforming a given function in its original time (space) domain to a frequency (wave number) domain and reversing it back. It computes the discrete Fourier transform (DFT) in an exceptionally efficient manner and saves significant CPU time and capacity.

For a given data function $F(t_n)$ with N samples, the DFT can be expressed as:

Forward:

$$\widehat{F}(\omega_k) = \sum_{n=0}^{N-1} F(t_n) e^{-i\omega_k t_n} \tag{3}$$

in which t_n is the discrete time sample, $\omega_k = 2\pi k/N$ is the discrete angular frequency and $k = 1, 2. ..,N - 1$.

Inverse:

$$F(t_n) = \frac{1}{N} \sum_{k=0}^{N-1} \widehat{F}(\omega_k) e^{i\omega_k t_n} \tag{4}$$

Standard FFT requires N to be a power of 2 and the sampling rate (time step) constant for the whole signal period. The latter constraint is adequate in many applications in engineering, but for solving heat transfer problems in GSHP systems, it can be restrictive. In this kind of systems, the designer is interested in the detailed thermal response of the GSHP at certain periods of switching ON and OFF the system, while at the same time needs to know its life time performance. If a detailed analysis with a sampling rate of one second is conducted for the life time of the system, which is typically 20 years, it would require more than 6.3×10^8 samples, which is practically unrealistic and can cause typical FFT numerical nuisances. If, on the other hand, an averaged analysis with a sampling rate of weeks or months is conducted, many important details on the hourly, daily and seasonal performance would be missing, making such analysis not representative of the real system. As such, the standard FFT can be useful to GSHP systems for either detailed analysis of relatively short periods, or averaged analysis of relatively long periods; not both at the same time.

The short time Fourier transform (STFT) is an elegant extension to the FFT, such that it enables dividing a time signal with a non-uniform frequency spectrum into segments, followed by computing the FFT for each segment separately [24]. The STFT, for segment j, can be expressed as:

Forward:

$$\widehat{F}^j(\omega_k) = \sum_{n=0}^{N-1} F^j(t_n) e^{-i\omega_k t_n} \tag{5}$$

Inverse:

$$F^j(t_n) = \frac{1}{N} \sum_{k=0}^{N-1} \widehat{F}^j(\omega_k) e^{i\omega_k t_n} \tag{6}$$

Standard STFT requires equal interval segments and constant sampling rate to all segments. These requirements are adequate in communication and audio processing [24], but for GSHP systems, it is likewise restrictive.

To tackle this issue, we make use of the STFT idea to divide the time signal into segments, but tailor it to analyze segments with different time intervals and different sampling rates. Basically, we divide the signal into segments, use FFT with different time stepping rates (starting from small to large time steps), solve the system, and then link the reconstructed time domain of these segments via the Heaviside function, as illustrated hereafter. The tailored FFT is expressed as:

Forward:

$$\widehat{F}^j(\omega_k^j) = \sum_{n=0}^{N^j-1} F^j(t_n^j) e^{-i\omega_k^j t_n^j} \tag{7}$$

where N^j is the number of samples for segment j with time step t_n^j, and ω_k^j is the discrete angular sampling frequency of segment j, expressed as:

$$\omega_k^j = \frac{2\pi k}{(N^j t_n^j)} \tag{8}$$

Inverse:

$$F^j(t_n^j) = \frac{1}{N^j} \sum_{k=0}^{N^j-1} \widehat{F}^j(\omega_k^j) e^{i\omega_k^j t_n^j} \tag{9}$$

Using the Heaviside function, the reconstructed time domain of the signal is described as

$$F(t_n) = \sum_j H(t_n - t_n^j) F^j(t_n^j) \tag{10}$$

This equation expresses the time domain of a signal composed of $\sum_j N^j$ segments, put together. The algorithm of the tailored FFT can be summarized in Algorithm 2:

Algorithm 2 (*Tailored FFT*).

1: DO $j = 1$ to J (*j*: the time segment)
2: Prescribe N^j, t_n^j
3: Apply Forward tailored FFT, Eq. (7)
4: Conduct STAND calculations
5: Apply Inverse tailored FFT, Eq. (9)
6: Aggregate the results with j − 1 segment, Eq. (10)
7: END DO

The tailored FFT will be applied in the numerical example given in Section 6 to highlight the capability of the model to tackle the short-to-long time problems.

4. Heat flow analysis based on heat pump power

As indicated earlier, the heat pump power cannot directly be prescribed as a heat flux to models which simulate heat flow in the U-tubes. Here, we derive an equation relating the heat pump power to the prescribed heat flux at the inlet of pipe-in, Eq. (A.7).

The power gained (lost) by the U-tube is expressed as

$$dP = \dot{m}\, c\, dT_{\mathrm{i}} \tag{11}$$

Considering $\dot{m} = \rho u A$ with A is the U-tube cross sectional area, Eq. (11) can be written as

$$dT_{\mathrm{i}} = \frac{1}{\rho\, c\, u A} dP \tag{12}$$

The Neumann boundary condition at the inlet of pipe-in, Eq. (A.7), is

$$q_{in} = -\lambda \frac{dT_i}{dz} A \tag{13}$$

where λ (W/(m K)) is the thermal conductivity of the circulating fluid. Substituting dT_i of Eq. (12) into Eq. (13), and re-arranging, gives

$$q_{in} dz = -\frac{\lambda}{\rho\, c\, u} dP \tag{14}$$

This equation entails that whether convective heat flux or conductive, the temperature at the inlet of the U-tube must be unique.

Integrating the left-hand side of this equation for a definite integral $0 \rightarrow 2L$ (with L being the BHE length, and $2L$ denoting the length of U-tube), and the right-hand side for $0 \rightarrow P$, leads to

$$q_{in} = -\frac{\lambda}{\rho\, c\, u} \frac{P}{2L} \tag{15}$$

which expresses the amount of heat transfer rate at the boundary of the U-tube when subjected to a heat pump power. The interplay between Eqs. (11) and (13) to produce Eq. (15) states that, in an adiabatic domain, the power gained by the U-tube (as a whole) is generated by a heat flux prescribed at the inlet of the U-tube. The heat flux at the boundary can be generated by any heat source, such as an electric heater or a heat pump.

As indicated above, Eq. (11) is valid for adiabatic processes, which occur without heat transfer between a thermodynamic system and its surrounding. Naturally, this is not the case for GSHP systems, as it is composed of multiple components and is in thermal contact with its surrounding soil mass. In mechanical engineering, the power of complex heat exchangers, such as those involving multiple tubes and shell passes, is calculated using a correction factor that implicitly incorporate the thermal interactions and losses among the heat exchanger components. Correction factors for several common configurations of mechanical heat exchangers are given in literature, see for example Pitts and Sissom [25]. Here, we apply a similar approach, by introducing a correction factor to Eq. (11), such that

$$dP = \varphi\, \dot{m}\, c\, dT_{\mathrm{i}} \tag{16}$$

where φ is a correction factor reflecting the non-adiabatic process of the GSHP, and can serve to cover any anomalies in measured data and description of physics. This implies that the inlet heat flux, Eq. (15), must be modified to read:

$$q_{in} = -\frac{\lambda}{\varphi\, \rho\, c\, u} \frac{P}{2L} \tag{17}$$

Normally, the heat pump power is not constant and varies with time due to electric voltage fluctuation and/or variation in its coefficient of performance (COP) [20], leading to:

$$q_{in}(t) = -\frac{\lambda}{\varphi\, \rho\, c\, u} \frac{P(t)}{2L} \tag{18}$$

This time dependent heat flux signal is implemented in the spectral analysis by first transforming it to the frequency domain and the resulted signal is applied to $\hat{q}_1$ on node 1 (Fig. A.2) on the right-hand side of Eq. (A.10).

To account for different BHE configurations, soil types and heat

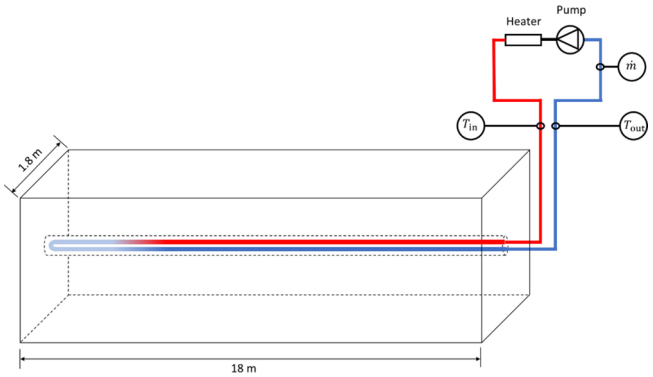

Fig. 2. A scheme of the prototype GSHP experiment, conducted by Beier et al. [26].

Table 1
Parameters of the prototype GSHP experiment [26].

Parameter	Value
Borehole length	18.3 m
Borehole diameter	0.126 m
Pipe outer diameter	0.0668 m
Pipe inner diameter	0.0547 m
Pipe thermal conductivity	0.39 W/(m K)
Soil thermal conductivity	2.82 W/(m K)
Grout thermal conductivity	0.73 W/(m K)
Average fluid volumetric flow rate	0.197 L/s
Average heat input rate	1056 W

pumps, we determine the GSHP correction factor numerically by calibrating the thermal power using Algorithm 3.

Algorithm 3 (*Tailored FFT & heat pump power prescription*).

1: DO $j = 1$ to J (j: the time segment)
2: Prescribe N^j, t_n^j
3: Transform the adiabatic form of the heat flux, Eq. (15), into the frequency domain and prescribe its magnitudes on node 1 in Eq. (A.10).
4: Conduct STAND calculations
5: Apply Inverse tailored FFT, Eq. (9)
6: Compute the power from Eq. (2)
7: Compare the specified heat pump power to the computed power, and calculate the correction factor, as
$\varphi = \frac{\text{Computed power}}{\text{Input power}}$
8: Insert the correction factor φ into Eq. (17)
9: Transform Eq. (17), into the frequency domain and prescribe its magnitudes on node 1 in Eq. (A.10).
10: Re-conduct the spectral analysis using STAND.
11: Apply the inverse tailored FFT, Eq. (9).
12: Aggregate the results with $j-1$ segment, Eq. (10)
13: END DO

In Section 5 we validate this approach with experimental results and in Section 6 we utilize it in the numerical examples.

5. Model verification

Beier et al. [26] presented a well-instrumented and documented experimental test set-up for a prototype ground source heat pump. They introduced experimental results and provided digital data for heat and fluid flow in a single U-tube, representing a borehole heat exchanger, embedded in a horizontal 1.8 m × 1.8 m × 18 m sandbox. The borehole is 18 m long, centered along the length of the box, Fig. 2. They used an electric heater as a heat source. A fluid circulates through the closed loop and its temperature is measured at the inlet and outlet of the loop every 1 min. A flow meter is used to measure the fluid flow rate through the loop. Details of the experimental test set-up can be found in their paper, referenced above. Table 1 lists the involved sandbox and borehole parameters.

Two experiments were conducted: a continuous heat pump operation; and an interrupted heat pump operation, in which the heat pump is switched OFF after 9 h for 2 h, followed by switching ON till the end of the experiment. Both experiments ran for about 50 h. Using the provided digital data, we reproduced the experimental results by applying two calculation approaches: calculation based on prescribed T_{in}, and calculation based on prescribed heat pump power.

5.1. Calculation based on prescribed T_{in}

Prescribing the temperature at the inlet of pipe-in is a common practice in analysing heat flow in GSHP systems (see for example [27]). In this calculation approach we set the measured temperature at the inlet of pipe-in as a prescribed T_{in} in the model, Eq. (A.8). Then, the temperature distributions along pipe-in, pipe-out and grout are calculated together with the temperature distribution in the surrounding soil mass. Fig. 3 shows the measured temperature at the inlet of pipe-in and the computed and measured temperatures at the outlet of pipe-out, for both experiments. The two plots in the figure show an excellent match

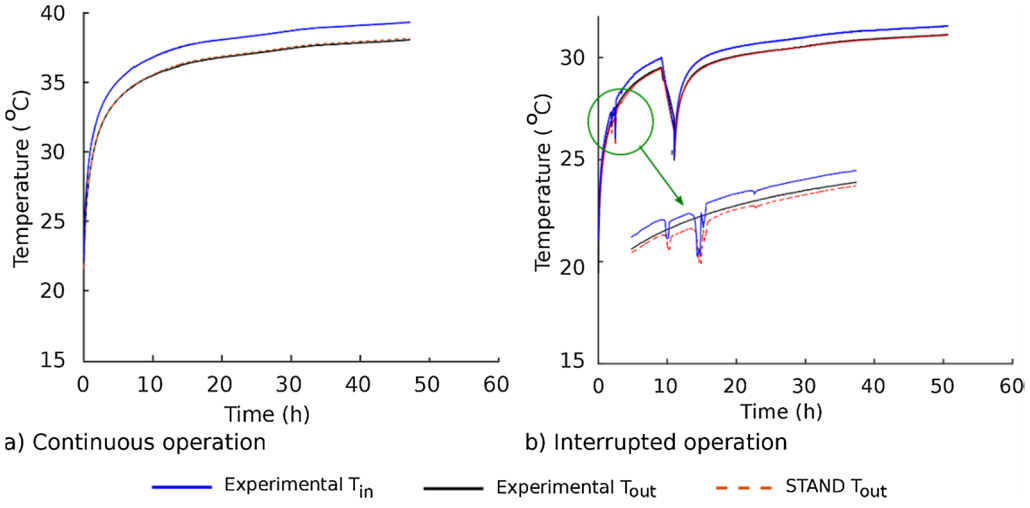

Fig. 3. Measured and computed temperature variations in time based on prescribed inlet temperature.

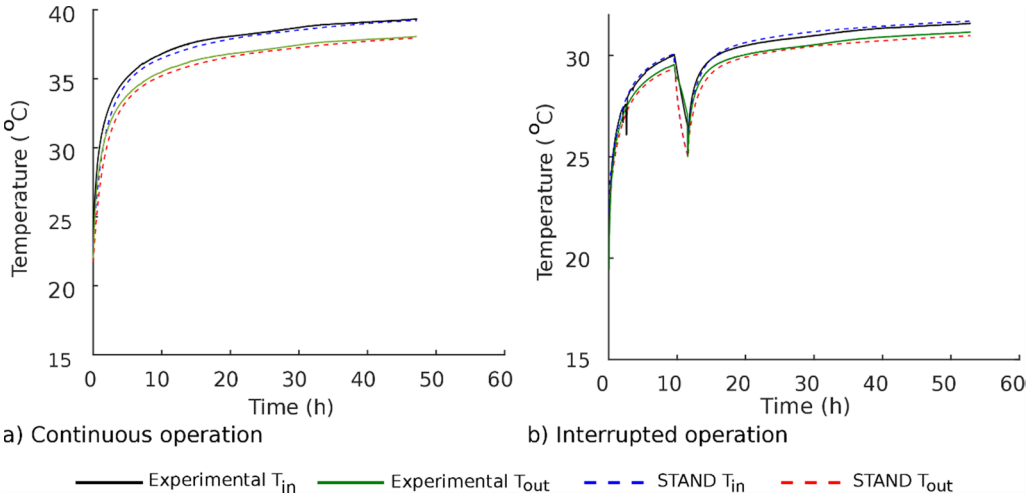

Fig. 4. Measured and computed temperature variations in time based on heat pump power.

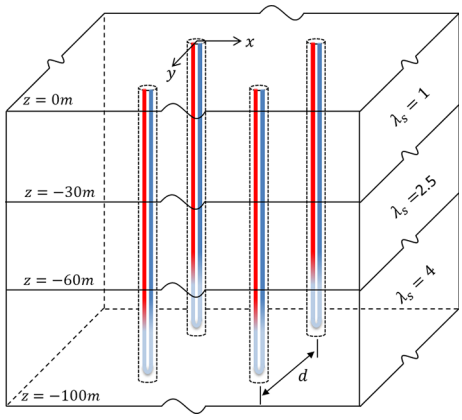

Fig. 5. A scheme of GSHP consisting of 4 BHEs embedded in 3 soil layers.

between the experimental and computed results. Equally, Fig. 3b demonstrates the capability of the model to simulate accurately the switching OFF and ON the system in the interrupted operation experiment.

It can be noted that the model could also detect the drop of the inlet temperature in the interrupted operation experiment, occurred between 1 and 5 h, see the zoomed image in Fig. 3b. The model properly captured its effect on the output temperature, but it is not clear why this drop in temperature has not been reflected in the measured outlet temperature.

5.2. Calculation based on heat pump power

Calculation based on the heat pump power is conducted using Algorithm 3 (Section 4). Using this calculation approach the temperature distribution in the whole system is computed, including T_{in}.

Fig. 4 shows the measured temperatures at the inlet of pipe-in and outlet of pipe-out, and their corresponding computed values for both experiments. The figure shows a good match between the experimental and computed results. Though, a closer look at the interrupted experiment reveals that the computed results overestimate $\Delta T(T_{in} - T_{out})$ by a maximum 0.3°C compared to the measured. This difference can be attributed to the error which might be introduced in calculating q_{in} in Eq. (18). Any variations in the measured fluid mass flow rate or deviations in the fluid density, specific heat and thermal conductivity can be reflected on the accuracy of q_{in} and hence on the computed temperature. Nevertheless, the correction factor accurately estimated the

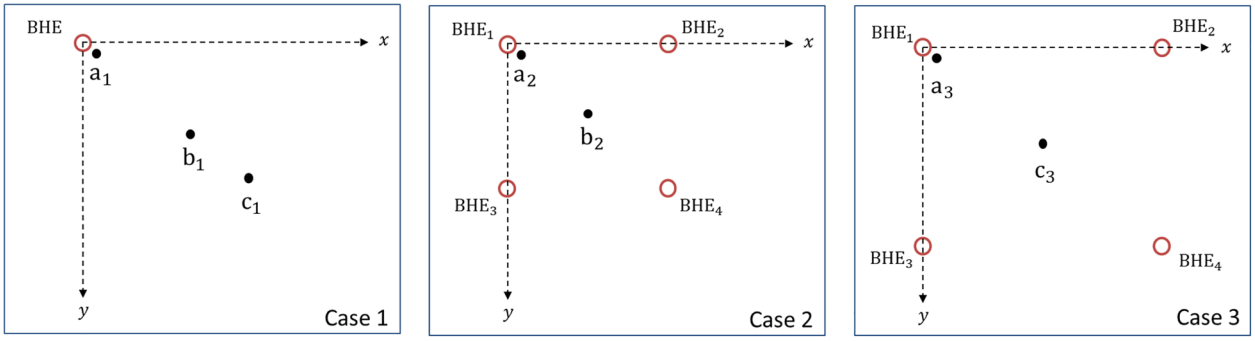

Fig. 6. Case 1: one active BHE; Case 2: four active BHEs, 5 m × 5 m; Case 3: four active BHEs, 8 m × 8 m.

Table 2
Material and geometrical parameters.

Parameter	Value	Parameter	Value
Borehole:		**Soil**:	
Borehole length	100 m	Film thickness	0.02 m
Borehole diameter	0.126 m	**Layer 1**: $0 \geq z \geq -30$ m	
Pipe external diameter	0.0547 m	Density, ρ_s	1100 kg/m^3
Pipe thermal conductivity	0.38 W/(m K)	Specific thermal capacity, c_s	1000 J/(kg K)
Fluid:		Thermal conductivity, λ_s	1. W/(m K)
Density, ρ	1050 kg/m^3		
Specific thermal capacity, c	3795 J/(kg K)	**Layer 2**: $-30 > z \geq -60$ m	
Thermal conductivity, λ	0.5 W/(m K)	Density, ρ_s	1500 kg/m^3
Dynamic viscosity, μ	0.0049 Pa s	Specific thermal capacity, c_s	1100 J/(kg K)
Velocity, u	0.5 m/s	Thermal conductivity, λ_s	2.5 W/(m K)
Grout:			
Density, ρ_g	1200 kg/m^3	**Layer 3**: $-60 > z \geq -100$ m	
Specific thermal capacity, c_g	2000 J/(kg K)	Density, ρ_s	1700 kg/m^3
Thermal conductivity, λ_g	1. W/(m K)	Specific thermal capacity, c_s	1200 J/(kg K)
		Thermal conductivity, λ_s	4. W/(m K)

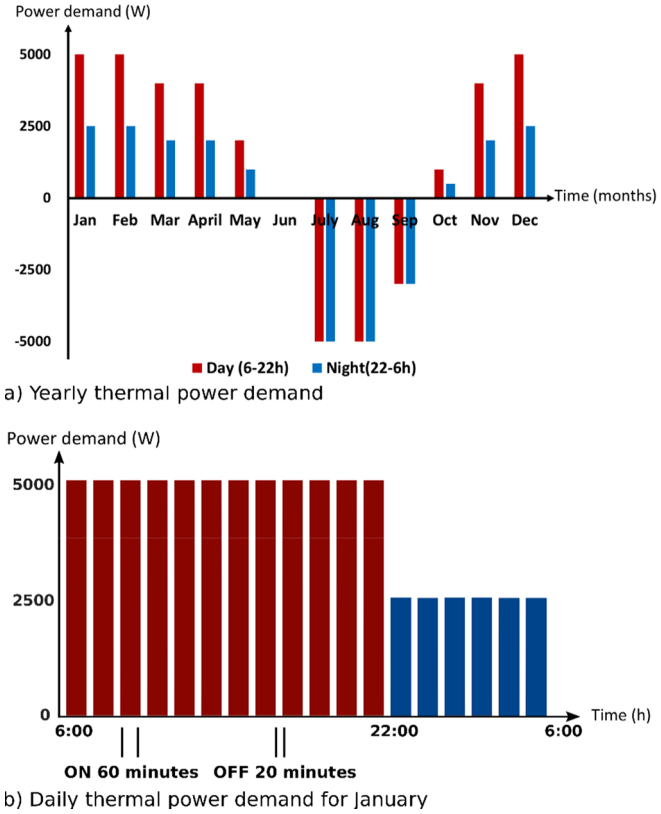

Fig. 7. Power demand from the ground.

anomalies in measured data and uncertainties in several parameters that resulted to good agreement between the experimental data and the computed temperatures at all stages: the transient at the beginning, the interrupted and the steady state.

6. Numerical examples

To demonstrate the model computational capability in simulating realistic cases, a numerical example illustrating heat flow in a typical ground source heat pump is introduced. A 2×2 BHE layout configuration constituting boreholes, 100 m in length, embedded in three soil layers exhibiting different thermal conductivities is simulated, Fig. 5. We studied three cases (Fig. 6):

Case 1: one active BHE;
Case 2: four active BHEs, 5 m $\times$ 5 m layout configuration (denoted as $d = 5$ m);
Case 3: four active BHEs, 8 m $\times$ 8 m layout configuration (denoted as $d = 8$ m).

The material and geometrical parameters of the system are given in Table 2. The initial temperature in all components is assumed 12 °C.

The heat pump works with varying power, depending on hourly, days and nights, and seasonal demands. Fig. 7a shows the power demand over the year, where it is assumed that this power represents the thermal energy gained from the heat pump, without the additional power usually gained from the compressor, neither the variations due to the COP of the heat pump.

The day starts at 6:00 (6 am) and ends at 22:00 (10 pm) and the night starts at 22:00 and ends at 6:00. Within these, the system is operating ON for 60 min and OFF for 20 min. Fig. 7b shows an example of the daily heat pump power for January. The year is divided into cold and warm months with varying thermal power demands. January till May, and October till December require heating; June requires neither heating nor cooling; and July till September are treated in two ways: with cooling (switching ON the heat pump in summer) and without cooling (switching OFF the heat pump in summer). The system is assumed to operate for 20 years. Any other operating scheme can also be considered.

The geometry is discretized using 3, 2-node spectral elements as schematically shown in Fig. A.2. The calculation is conducted using the tailored FFT with a multiple time stepping scheme, as the following:

Day 1:	time step = 1 s.
Day 2 – end of Year 1:	time step = 5 min.
Year 2 – end of Year 20:	time step = 24 h.

This scheme entails a very detailed analysis in the first day, a detailed analysis in the first year and a daily-averaged analysis for the rest. Other schemes can also be conducted, depending on the required details.

As indicated earlier, the model is capable of calculating the temperature distributions in all BHE components and in the soil mass in an

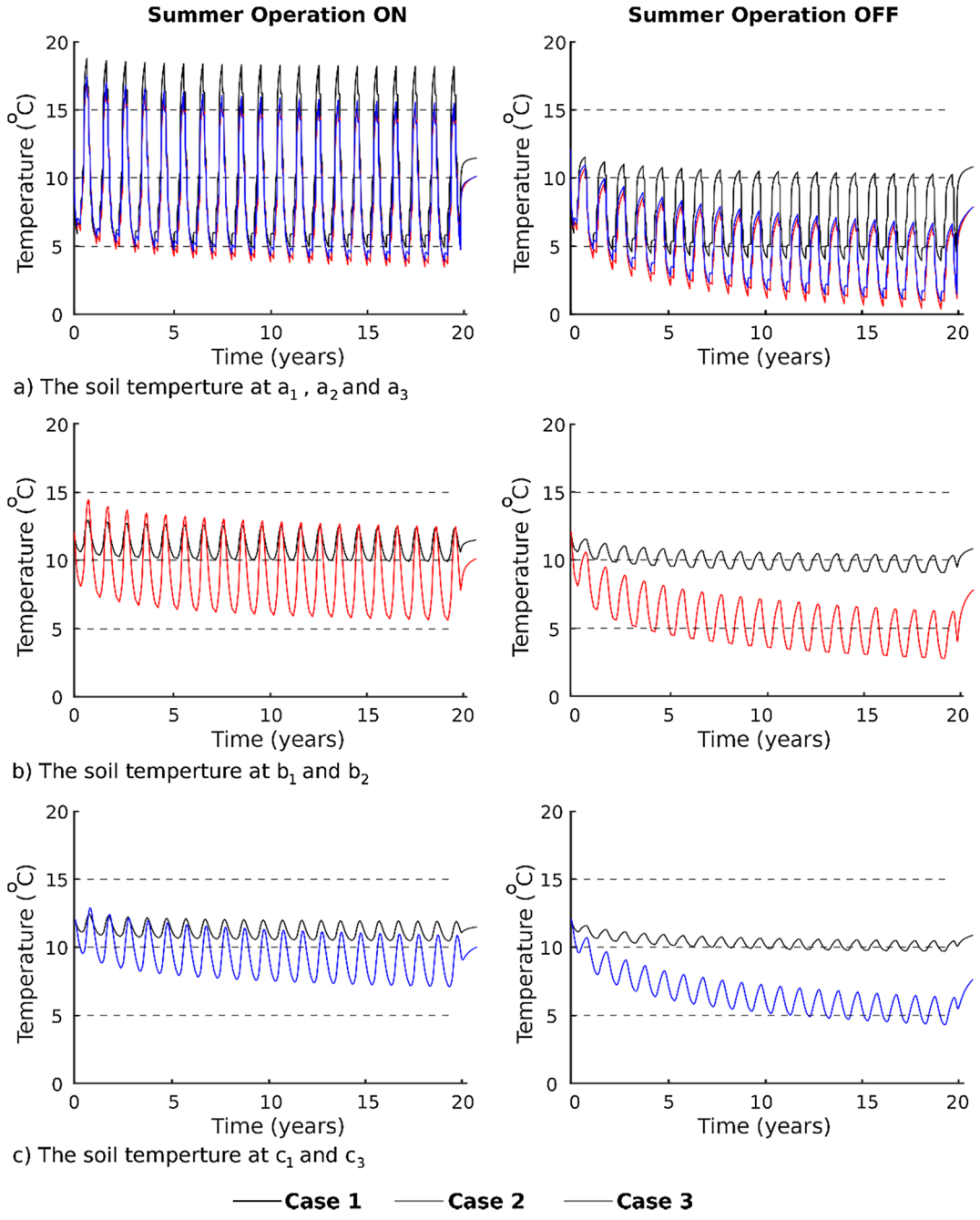

Fig. 8. Soil temperature at $z = 100$ m for Case1, Case 2 and Case 3.

effectively 3D space. Using the heat pump power option, even the temperature at the inlet of pipe-in, T_{in}, is calculated.

Fig. 8 shows the soil temperature distributions for the 3 cases:

Case 1: One BHE is operating (Fig. 6) in two options: cooling ON in summer, and cooling OFF in summer. The temperature is computed at a_1 (0.1, 0.1), b_1 (2.5, 2.5) and c_1 (4, 4). The computed results for these three points are shown in Fig. 8a, Fig. 8b, and Fig. 8c, respectively.

Case 2: Four BHEs with 5 m × 5 m layout configuration (i.e. = 5 m, Figs. 5 and 6) in two options: cooling ON in summer, and cooling OFF in summer. The temperature is computed at a_2 (0.1, 0,1) and b_2 (2.5, 2.5). The computed results for these two points are shown in Fig. 8a and Fig. 8b, respectively.

Case 3: Four BHEs with 8m × 8m layout configuration (i.e. d= 8m , Figs. 5 and 6) in two options: cooling ON in summer, and cooling OFF in summer. The temperature is computed at a_3 (0.1, 0,1) and c_3 (4, 4). The computed results for these two points are shown in Fig. 8a and Fig. 8b, respectively.

Fig. 8 clearly shows the effect of boreholes interactions on the soil temperature. At a short distance from the boreholes (a_1, a_2 and a_3) the

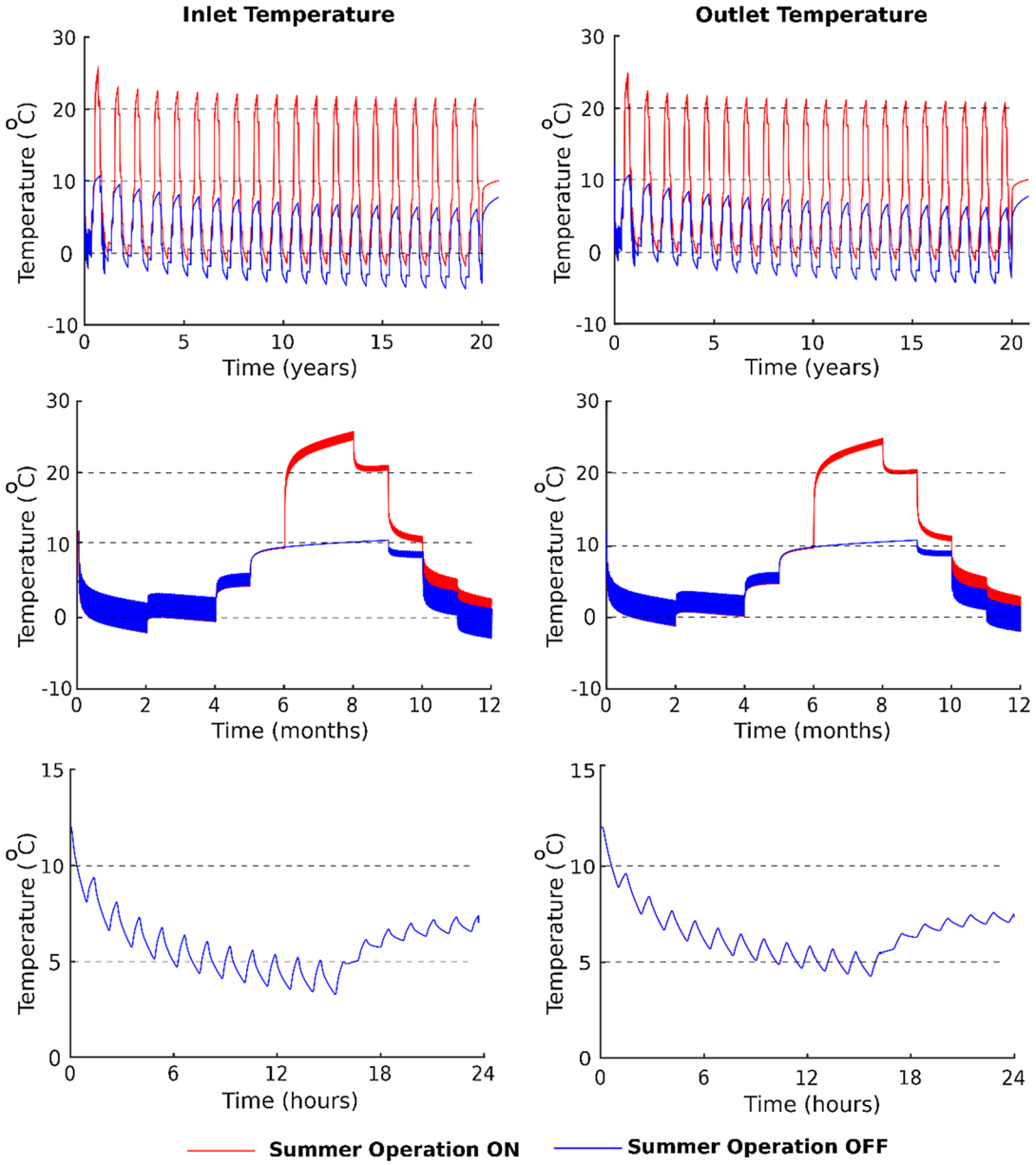

Fig. 9. Inlet and outlet temperatures for Case 2.

soil temperature in the three cases is nearly the same for the cooling ON option, but for the cooling OFF, Cases 2 and 3 have clearly been affected. The soil temperature in these two cases is 3 °C lower than if only one BHE is operating after 20 years of operation.

At relatively far distances from the BHE, b_1, b_2, c_1 and c_3, the effect of the borehole interactions are obvious. For Case 2, at point b_2, the temperature difference after 20 years of operation between a single BHE and 4 BHEs is 4.3 °C for the cooling ON option, and 7.0 °C for the cooling OFF. For Case 3, at point c_3, the temperatures were 3.3 °C and 5.4 °C, respectively.

Fig. 8 also shows that the space between BHEs in a grid of neighbouring boreholes has a significant impact on the soil temperature. Likewise, cooling in summer is important for the soil mass to recover its thermal storage capacity.

Fig. 9 shows the computed temperature variations for Case 2 at the inlet of pipe-in (T_{in}) and outlet of pipe-out (T_{out}) for two options: cooling ON in summer; and cooling OFF in summer. The figure shows the computed results for 20 years, together with the zoomed results for the first year and first day. These results demonstrate the computational capability of the model to calculate the detailed performance of the system for short periods, and its performance for long period, all done in a single run.

Fig. 9 also shows an important physical observation. Operating the geothermal system for cooling in summer helps the ground to recover its heat and thus makes the system more sustainable. This observation has been discussed in detail by Zhao et al. [28]. In this specific case, the decline of temperature between year 1 and year 20 for the cooling ON is 1.8 °C, but for the cooling OFF, it is 4.9 °C.

Fig. 10 shows the vertical temperature distributions for Case 2 in pipe-in, pipe-out, grout and soil at a_2 and b_2 in February and August of year 1, and those in year 20. The summer cooling is ON. The figure shows the model capability to simulate the detailed effects of the soil thermal conductivity on the thermal propagation and contraction at different months of the year.

Fig. 11 shows the soil temperature snapshots at a 10 m × 10 m cross-sectional area surrounding the bottom of the boreholes

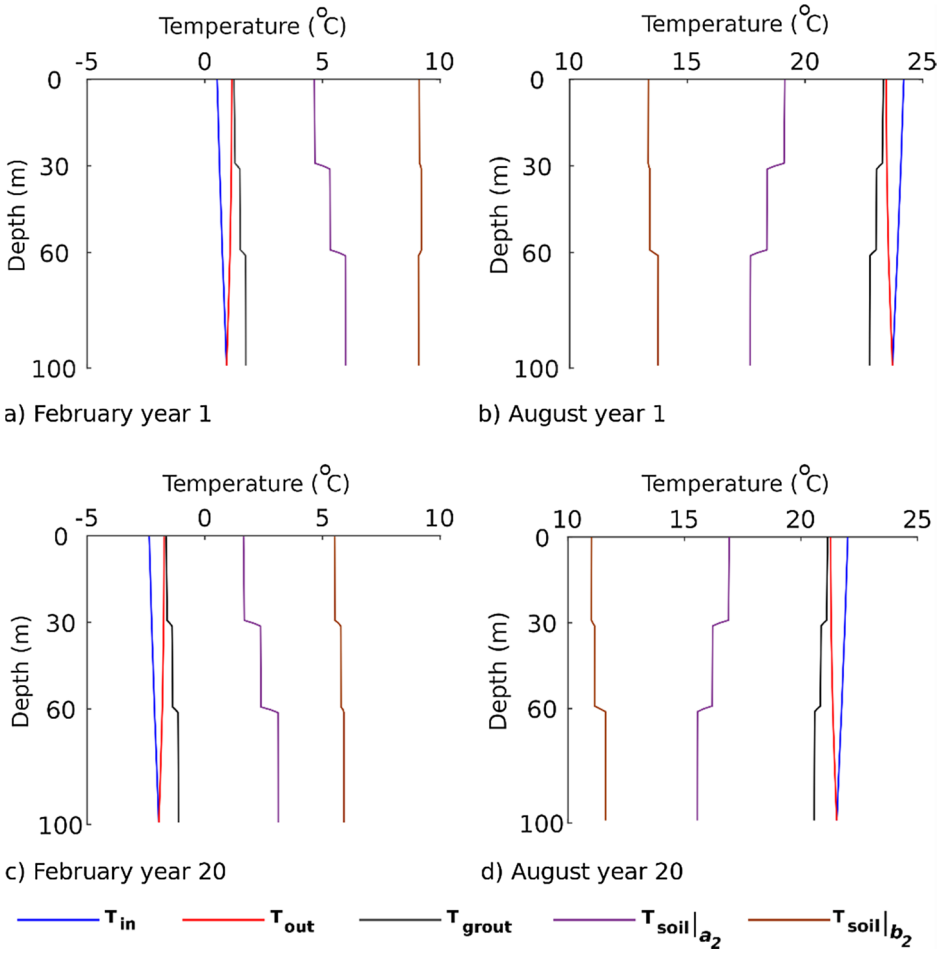

Fig. 10. Vertical temperature distributions in pipe-in, pipe-out, grout and soil for Case 2.

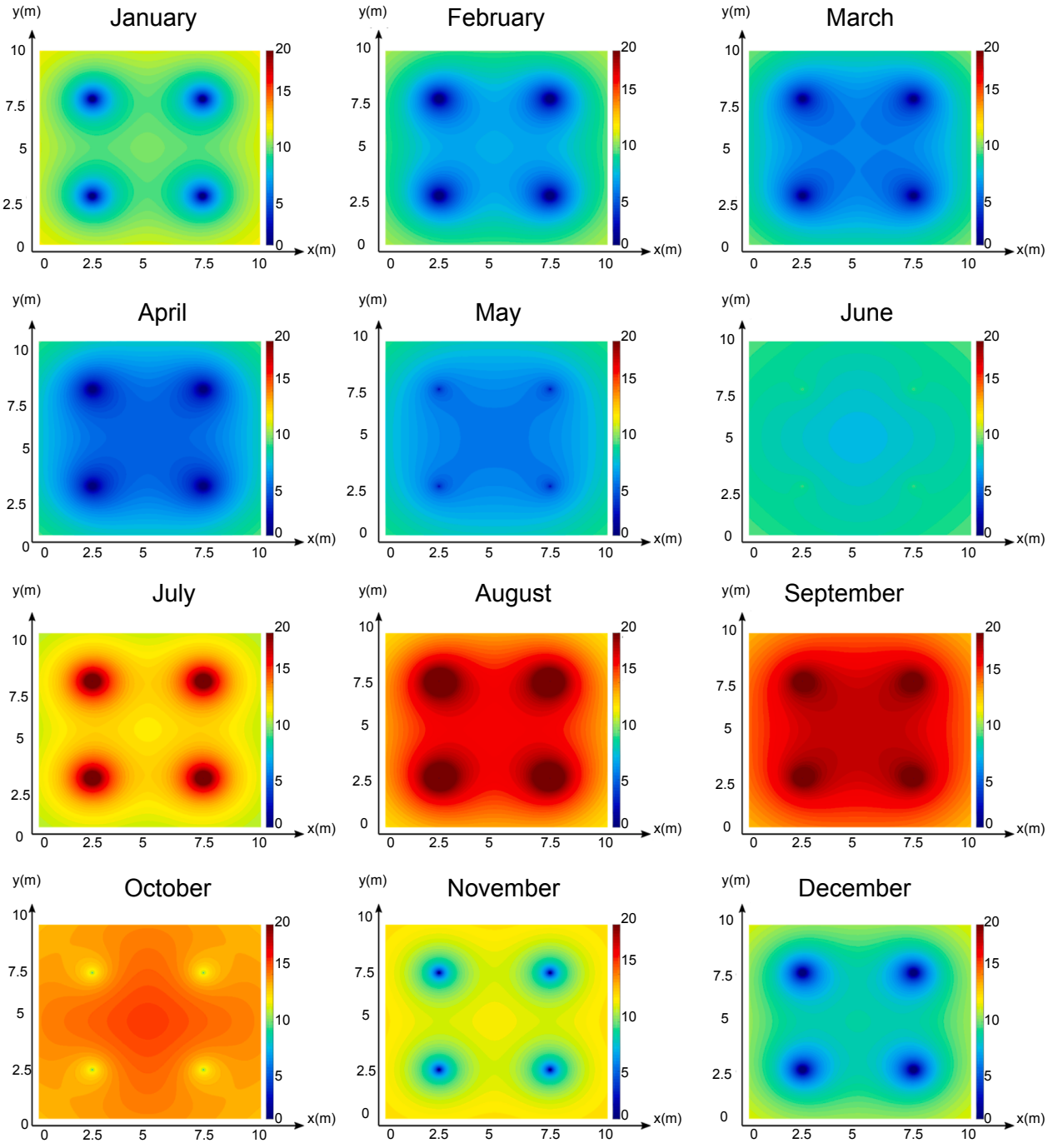

Fig. 11. Soil temperature snapshots at $z = 100$ m for Case 2.

($z = 100$ m) on the last day of the month, in the first 12 months of operation. The figure clearly shows the thermal interaction between boreholes and their effects on the soil mass at different times of the year.

It is worth mentioning here that although the model for a single borehole is axisymmetric, the use of the superposition principle has produced a significant spatial imbalance in the soil temperature distribution. However, by definition, the 2×2 BHE layout produces symmetric heat extraction rate for all BHEs. Any other layout such as 3×3 BHE or random distribution would produce unsymmetrical heat extraction rates. Kurevija et al. [29], Gultekin et al. [30] and You et al. [31] have discussed this issue in detail. This topic will be the focus of a coming publication.

7. Conclusions

This paper introduces a semi-analytical model for simulating heat flow in ground source heat pump systems, with emphasis on simulating short-to-long term heat flow using the heat pump power as input. The essential features of the model are:

1. It solves heat flow in effectively 3D geometries for any required temporal details. Detailed system operation from seconds to years can be handled in a single run. Hourly, daily and seasonally switching ON and OFF can be considered in the calculation.
2. It solves the system of equations using the heat pump power directly. Although in literature there are several models making use of the heat pump power to solve the system, they end up prescribing the Dirichlet boundary condition (T_{in}) at the inlet of the U-tube. Here, we prescribe the Neumann boundary condition (q_{in}), derived from the heat pump power. The Neumann boundary condition allows using the heat pump power directly, but would be realistic if the COP and the compressor effect are taken into consideration. This subject will be the focus of a future work.

Physically, the numerical example demonstrates that operating the heat pump in summer (i.e. cooling ON mode) helps the earth to recover its temperature, and hence increases the GSHP thermal efficiency.

Declaration of Competing Interest

There is no conflict of interest.

Appendix A. Governing equations

The governing heat equations of a ground source heat pump consisting of a single U-tube borehole heat exchanger embedded in a soil mass, Fig. A.1, can be described as

Pipe-in

$$\rho c\frac{\partial T_i}{\partial t}dV_i - \lambda\frac{\partial^2 T_i}{\partial z^2}dV_i + \rho cu\frac{\partial T_i}{\partial z}dV_i + b_{ig}(T_i - T_g)dS_{ig} = 0 \tag{A.1}$$

Pipe-out

$$\rho c\frac{\partial T_o}{\partial t}dV_o - \lambda\frac{\partial^2 T_o}{\partial z^2}dV_o - \rho cu\frac{\partial T_o}{\partial z}dV_o + b_{og}(T_o - T_g)dS_{og} = 0 \tag{A.2}$$

Grout

$$\rho_g c_g\frac{\partial T_g}{\partial t}dV_g - \lambda_g\frac{\partial^2 T_g}{\partial z^2}dV_g + b_{ig}(T_g - T_i)dS_{ig} + b_{og}(T_g - T_o)dS_{og} + b_{gs}(T_g - T_s)dS_{gs} = 0 \tag{A.3}$$

Soil film

$$\rho_s c_s\frac{\partial T_s}{\partial t}dV_s - \lambda_s\frac{\partial^2 T_s}{\partial z^2}dV_s + b_{gs}(T_s - T_g)dS_{gs} + b_{ss}(T_s - T_{\text{soil}})dS_s = 0 \tag{A.4}$$

Soil mass

$$\frac{1}{\alpha}\frac{\partial T_{\text{soil}}}{\partial t} - \frac{\partial^2 T_{\text{soil}}}{\partial r^2} - \frac{1}{r}\frac{\partial T_{\text{soil}}}{\partial r} = 0 \tag{A.5}$$

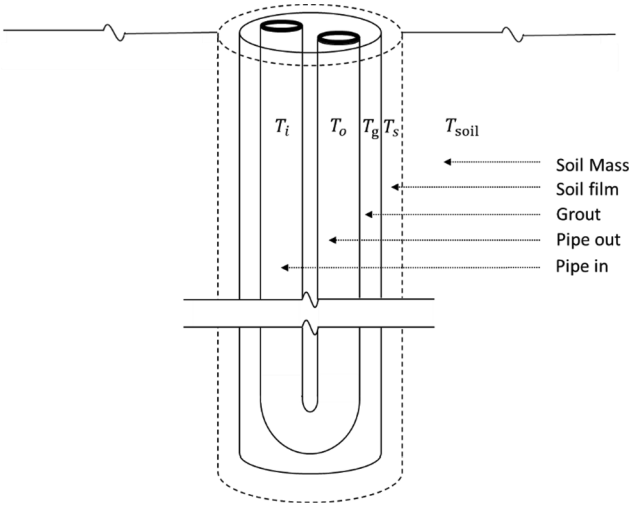

Fig. A1. A schematic representation of a single U-tube BHE and its surrounding soil mass.

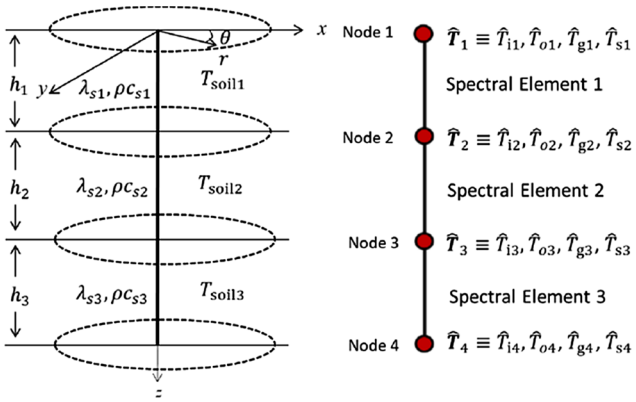

Fig. A2. A three-layer system and its spectral element discretization.

where the subscripts i, o, g and s represent pipe-in, pipe-out, grout and soil film, respectively; and $T_i = T_i(z, t)$, $T_o = T_o(z, t)$, $T_g = T_g(z, t)$, $T_s = T_s(z, t)$ and $T_{soil} = T_{soil}(r, t)$ are the temperatures in pipe-in, pipe-out, grout, soil film and soil mass, respectively. λ, λ_g and λ_s (W/(m K)) are the thermal conductivity of the circulating fluid, grout and soil film, respectively; u (m/s) is the circulating fluid velocity; b_{ig}, b_{og}, b_{gs}, b_{ss} (W/(m^2 K)) are the thermal interaction coefficients between pipe in-grout, pipe out-grout, grout-soil film, and soil film-soil mass, respectively; ρc (J/(m^3 K)) is the volume heat capacity, with c (J/(kg K)) the specific heat capacity and ρ (kg/m^3) the mass density; dV_i, dV_o, dV_g, dV_s (m^3) are the control volumes of pipe-in, pipe-out, grout and soil film, respectively, and dS_{ig}, dS_{og}, dS_{gs}, dS_s(m^2) are their associated surface areas; and α(m^2/s) is the thermal diffusivity of the soil.

The soil film (Eq. (A.4)) is introduced in this model to couple the borehole heat exchanger to the soil mass. Details of this issue is thoroughly covered in BniLam and Al-Khoury [6] and BniLam et al. [5].

The initial condition is

$$T_i(z,\ 0) = T_o(z,\ 0) = T_g(z,\ 0) = T_s(z,\ 0) = T_{soil}(r,\ 0) \tag{A.6}$$

The boundary condition at the inlet of pipe-in might be any of two types:
a Neumann boundary condition:

$$q_i(0,\ t) = q_{in}(t) = -\lambda \frac{dT_i}{dz} dA_i \tag{A.7}$$

or a Dirichlet boundary condition:

$$T_i(0,\ t) = T_{in}(t) \tag{A.8}$$

where q_{in} is the heat flux and T_{in} is the prescribed inlet temperature, that might have any arbitrary distribution in time.

This initial and boundary value problem is solved using the spectral element method [32,20]. This method combines the analytical solution for a homogeneous domain to the finite element matrix assembly technique for a heterogeneous domain. The resulting spectral element equation is similar to the algebraic finite element equation, such that

$$\mathbf{K}(\omega_n)\hat{\mathbf{T}} = \hat{\mathbf{q}} \tag{A.9}$$

in which $\mathbf{K}(\omega_n)$ represents the spectral element matrix, in resemblance to that of the finite element stiffness matrix, but here it is exact and frequency-dependent; $\hat{\boldsymbol{T}}$ is the nodal temperature vector and $\hat{\boldsymbol{q}}$ is the nodal heat flux vector.

For a multilayer system, each layer is described by a spectral element. The assembly of the global matrix is done following the finite element method. If, for example, we have a borehole heat exchanger embedded in a three layer soil mass, shown schematically in Fig. A.2, the system is discretized by three spectral elements and four nodes. Each node has four degrees of freedom, describing the temperatures in pipe-in, $\hat{T}_i$, pipe-out, $\hat{T}_o$, grout, $\hat{T}_g$, and soil film, $\hat{T}_s$. The stiffness matrix for each element is described by Eq. (A.9). Using the finite element mesh assembling technique, the global spectral element equation can then be described as

$$\begin{bmatrix} \boldsymbol{K}_{11}^1 & \boldsymbol{K}_{12}^1 & & \\ \boldsymbol{K}_{21}^1 & K_{22}^1 + \boldsymbol{K}_{11}^2 & \boldsymbol{K}_{12}^2 & \\ & \boldsymbol{K}_{21}^2 & \boldsymbol{K}_{22}^2 + \boldsymbol{K}_{11}^3 & \boldsymbol{K}_{12}^3 \\ & & \boldsymbol{K}_{21}^3 & \boldsymbol{K}_{22}^3 \end{bmatrix} \begin{bmatrix} \hat{\boldsymbol{T}}_1 \\ \hat{\boldsymbol{T}}_2 \\ \hat{\boldsymbol{T}}_3 \\ \hat{\boldsymbol{T}}_4 \end{bmatrix} = \begin{bmatrix} \hat{\boldsymbol{q}}_1 \\ \hat{\boldsymbol{q}}_2 \\ \hat{\boldsymbol{q}}_3 \\ \hat{\boldsymbol{q}}_4 \end{bmatrix} \tag{A.10}$$

in which the matrix on the left-hand side is the global stiffness matrix, with the superscript indices indicating the element (layer) number. The vector on the left-hand side is the degrees of freedom vector, indicating the nodal temperatures that need to be determined; and the vector on the right-hand side is the corresponding nodal heat fluxes. Readers interested in the formulation of the spectral elements for a multilayer GSHP systems are referred to BniLam et al. [23].

References

[1] Horizon2010 Projects: https://www.geothermalresearch.eu/active-geothermalprojects/horizon2020-projects/ (accessed August 2019).
[2] Y. Cui, J. Zhu, S. Twaha, S. Riffat, A comprehensive review on 2D and 3D models of vertical ground heat exchangers, Renew. Sustain. Energy Rev. 94 (2018) 84–114.
[3] COMSOL 5.4: https://www.comsol.nl/ (accessed August 2019).
[4] FEFLOW: https://www.mikepoweredbydhi.com/products/feflow/geothermalenergy (accessed August 2019).
[5] ABAQUS: https://www.simuleon.com/simulia-abaqus/?gclid=Cj0KCQiA_4jgBRDhARIsADezXcjJk3jv5su_vcd0zbAWU4EP1vfL8K302zdoHkhKyHgkP-ktftb1IaAp7aEALw_wcB (accessed August 2019).
[6] K. Pruess, C. Oldenburg, G. Moridis, "TOUGH2 User's Guide, Version 2.0", Lawrence Berkeley National Laboratory Report LBNL-43134, Berkeley, CA, November 1999.
[7] D. Marcotte, P. Pasquier, Fast fluid and ground temperature computation for geothermal ground-loop heat exchanger systems, Geothermics 37 (2008) 651–665.
[8] L. Zhang, G. Huang, Q. Zhang, J. Wang, An hourly simulation method for the energy performance of an office building served by a ground-coupled heat pump system, Renew. Energy 126 (2018) 495–508.
[9] J. Claesson, S. Javed, An analytical method to calculate borehole fluid temperatures for time-scales from minutes to decades, ASHRAE Trans. 117 (2) (2011) 279–288.
[10] M. Li, P. Li, V. Chan, A.C.K. Lai, Full-scale temperature response function (G-function) for heat transfer by borehole ground heat exchangers (GHEs) from sub-hour to decades, Appl. Energy 136 (2014) (2014) 197–205.
[11] M. Li, K. Zhu, Z. Fang, Analytical Methods for Thermal Analysis of Vertical Ground Heat Exchangers, Woodhead Publishing Edition. Woodhead Publishing Series in Energy, Rees, Simon, 2016, pp. 157–183.
[12] H.S. Carslaw, J.C. Jaeger, Conduction of Heat in Solids, second ed., Oxford University Press, London, UK, 1959.
[13] R. Al-Khoury, T. Kölbel, R. Schramedei, Efficient numerical modeling of borehole heat exchangers, Comput. Geosci. 36 (10) (2010) 1301–1315.
[14] T.Y. Ozudogru, C.G. Olgun, A. Senol, 3D numerical modeling of vertical geothermal heat exchangers, Geothermics 51 (2014) 312–324.
[15] R. Yi, G. Denis, Y. Mei, Modelling ground source heat pump system by an integrated simulation programme, Appl. Therm. Eng. 134 (2018) (2018) 450–459.
[16] EED v4: https://buildingphysics.com/eed-2/ (accessed August 2019).
[17] P. Eskilson, Thermal Analysis of Heat Extraction Boreholes Doctoral Thesis, University of Lund, Department of Mathematical Physics, Lund, Sweden, 1987.
[18] GLHEPRO v5: https://hvac.okstate.edu/glhepro/overview (accessed August 2019).
[19] J.D. Spitler, GLHEPRO – a design tool for commercial building ground loop heat exchangers, Proceedings of the Fourth International Heat Pumps in Cold Climates Conference, (2000).
[20] R. Al-Khoury, Computational Modeling of Shallow Geothermal Systems, CRC Press/Taylor & Francis Group, 2012.
[21] N. BniLam, R. Al-Khoury, Transient heat conduction in an infinite medium subjected to multiple cylindrical heat sources: an application to shallow geothermal systems, Renew. Energy 97 (2016) 145–154.
[22] N. BniLam, R. Al-Khoury, A spectral element model for nonhomogeneous heat flow in shallow geothermal systems, Int. J. Heat Mass Transfer 104 (2017) 703–717.
[23] B. Noori, A.-K. Rafid, S. Arsha, L.J. Sluys, A semi-analytical model for detailed 3D heat flow in shallow geothermal systems, Int. J. Heat Mass Transfer 123 (2018) 911–927.
[24] A. Mertins, Signal Analysis: Wavelets, Filter Banks, Time-Frequency Transforms and Applications, John Wiley & Sons Ltd., 1999.
[25] D.R. Pitts, L.E. Sissom, Schaum's Outline of Heat Transfer, second ed., Mc-Graw-Hill, Singapore, 1997.
[26] R.A. Beier, M.D. Smith, J.D. Spitler, Reference data sets for vertical borehole ground heat exchanger models and thermal response test analysis, Geothermics 40 (1) (2011) 79–85.
[27] B. Marcotte, M. Bernier, Experimental validation of a TRC model for a double U-tube borehole with two independent circuits, Appl. Therm. Eng. 162 (2019).
[28] Z. Zhongchao, S. Rendong, F. Weixian, Z. Yong, Z. Yanrui, Soil Thermal Balance analysis for a ground source heat pump system in a hot-summer and cold-winter region, Energies 2018 (11) (2018) 1206.
[29] T. Kurevija, D. Vulin, V. Krapec, Effect of borehole array geometry and thermal interferences on geothermal heat pump system, Energy Convers. Manage. 60 (2012) 134–142.
[30] A. Gultekin, M. Aydin, A. Sisman, Thermal performance analysis of multiple borehole heat exchangers, Energy Convers. Manage. 122 (2016) 544–551.
[31] T. You, X. Li, S. Cao, H. Yang, Soil thermal imbalance of ground source heat pump systems with spiral-coil energy pile groups under seepage conditions and various influential factors, Energy Convers. Manage. 178 (2018) 123–136.
[32] J.F. Doyle, Wave Propagation in Structures: Spectral Analysis Using Fast Discrete Fourier Transforms, Springer-Verlag, New York, 1997.